Von Kármán vortex streets on the sphere

Cite as: Phys. Fluids **21**, 116603 (2009); https://doi.org/10.1063/1.3258066
Submitted: 28 July 2009 . Accepted: 07 October 2009 . Published Online: 20 November 2009

George Chamoun, Eva Kanso, and Paul K. Newton

Von Kármán vortex streets on the sphere

George Chamoun, Eva Kanso, and Paul K. Newton[a)]
Aerospace and Mechanical Engineering, University of Southern California, 854 Downey Way, Los Angeles, California 90089-1191, USA

(Received 28 July 2009; accepted 7 October 2009; published online 20 November 2009)

We consider streamline patterns associated with single and double von Kármán point vortex streets on the surface of a nonrotating sphere, with and without pole vortices. The full family of streamline patterns are identified and the topological bifurcations from one pattern to another are depicted as a function of latitude and pole strength. The process involves first finding appropriate vortex strengths so that the configuration forms a relative equilibrium, then calculating the angular rotation of the configuration about the center-of-vorticity vector. We move in a rotating frame of reference so that the configuration is fixed, identify the separatrices in the flowfield, and plot the global streamline patterns as a function of the pole strengths and latitudinal positions of the rings. We carry the procedure out for single and double von Kármán vortex streets, with and without pole vortices. The single von Kármán street configurations are comprised of n evenly spaced vortices on each of two rings that symmetrically straddle the equator and are skewed with respect to each other by half a wavelength, while the double von Kármán ring configurations are made up of four rings of n evenly spaced vortices symmetrically straddling the equator. © *2009 American Institute of Physics*. [doi:10.1063/1.3258066]

I. INTRODUCTION

A. Preliminaries

This paper considers streamline patterns generated by single and double von Kármán point vortex streets[1] on the surface of a sphere, with and without pole vortices, the simplest of which is shown schematically in Fig. 1. The figure depicts $n=6$ point vortices evenly distributed on an upper fixed latitudinal ring, and six vortices on a lower ring symmetrically placed across the equator, skewed by half a wavelength with respect to the upper street. That is, there is a total of $N=2n=12$ point vortices in the configuration. The positions of the point vortices are given in Cartesian variables by $\mathbf{x}_\alpha, (\alpha=1,\ldots,12)$, where $\|\mathbf{x}_\alpha\|=1$. Each of the point vortices on the upper ring has strength $\Gamma \in \mathbb{R}$ (with Γ positive in the counter-clockwise direction), each on the lower ring has opposite strength $-\Gamma$, and as a result, the center-of-vorticity vector $\mathbf{J}=\Sigma_{i=1}^{N}\Gamma_\alpha \mathbf{x}_\alpha$ is aligned with the north-south polar axis and the system rotates with angular frequency ω_N around it. When pole vortices are included, they are equal and opposite in strength and then the total number of point vortices is $N=2n+2$.

We know from the work of Ref. 2 that von Kármán configurations form in planetary atmospheres and their streamline topologies can vary depending on aspect ratio and latitude. From, Ref. 3 we know that the presence of pole vortices can and do play an important role in stabilizing or destabilizing a given latitudinal configuration. We also know from the work of Refs. 4 and 5 that the streamline patterns associated with fixed and relative equilibria on the sphere determine key properties of mixing and global transport. The recent comprehensive paper[6] is an excellent account of the relation between streamline topologies in fluid flow and their ramifications. See also Ref. 7 for applications of these ideas to the near wake of a circular cylinder. Our main motivation in this paper is to flesh out the full range of streamline patterns that are obtained with von Kármán configurations as a function of ring latitude and pole strength, in order to better contextualize the patterns recently identified and studied in Jupiter's atmosphere, as described in papers.[2,8–10] In these works, three main patterns were identified, called type I, II, and III (see Fig. 3 of Ref. 2). We will show how these patterns arise as a function of our bifurcation parameters, and that these patterns are actually only a small subset of all possible patterns that such configurations can, in principle, generate. We mention other related works on relative equilibrium ring formations of point vortices on the sphere, Refs. 11 and 12. The latter, among other things, considers skewed rings of equal and opposite signed vortices—what we call the single von Kármán street (VKS). Other recent related work on equilibria of distributed vorticity regions on the sphere include Ref. 13 (there is a parametric limit in which the distributed vortices reduce to point vortices) and Ref. 14, as well as enlightening papers on the emergence and dynamics of vortices in numerical simulations on the sphere, Refs. 15 and 16.

Understanding the streamline patterns generated by systems of von Kármán vortex streets on the sphere involves three distinct steps which we carry out in this paper:

(1) Given a configuration of point vortices on the (unit) sphere arranged in a von Kármán pattern, find the allowable vortex strength vector $\mathbf{\Gamma} \in \mathbb{R}^N$ that renders the system a relative equilibrium configuration which rotates about the north-south polar axis.
(2) Find the rotational frequency associated with the relative equilibrium.

a)Author to whom correspondence should be addressed. Electronic mail: newton@usc.edu.

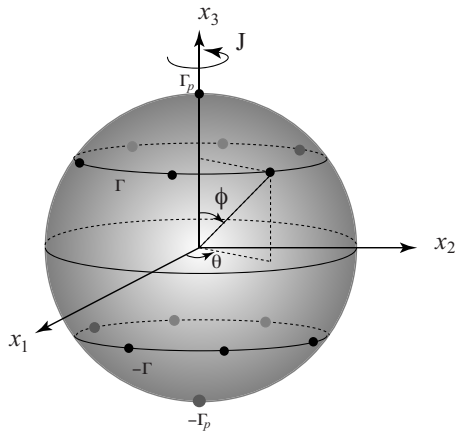

FIG. 1. Schematic of a single VKS on the sphere with an illustration of the vorticity vector **J** where the upper ring is placed at colatitude ϕ. N is the total number of vortices, n is the number of vortices per ring, hence $N=2n$. When pole vortices are included, we have $N=2n+2$.

(3) Move in a rotating frame to render the configuration a fixed equilibrium, and identify the separatrices and streamline topologies in this frame. For this, we need to identify all the hyperbolic and elliptic stationary points on the sphere in addition to those located at the actual point vortex positions.

The streamline patterns depend on (i) the latitudes at which the rings comprising the streets sit, (ii) how many streets straddle the equator, and (iii) whether or not there is pole vorticity. The results are topological in nature, meaning they depend on the number of centers and saddles in the vectorfield, not, in general, on details of how the vorticity is distributed. We mention, up front, a basic tool in understanding streamline patterns on the sphere: the index theorem of Poincaré.

Theorem (PIT). The index $I_f(S)$ of a two-dimensional surface S relative to any C^1 vector field f on S with at most a finite number of critical points is equal to the Euler–Poincaré characteristic of S, denoted $\chi(S)$, i.e., $I_f(S)=\chi(S)$.

We know for a sphere, $\chi(S)=2$. The index for a center is $+1$, while that for a saddle is -1. Hence if c denotes the number of centers present (point vortices plus other centers) and s denotes the number of saddles, then one has $c-s=2$. Thus, all of the streamline patterns produced must respect this constraint, which gives a nice check on the consistency of the patterns produced. See Refs. 4 and 5 for more on applications of the PIT to the understanding of streamline patterns on the sphere.

B. Equations of motion

The evolution equations for N-point vortices moving on the surface of a nonrotating unit sphere, written in Cartesian coordinates, are given in Ref. 17:

$$\dot{\mathbf{x}}_\alpha = \frac{1}{4\pi}\sum_{\beta=1}^{N}{}'\Gamma_\beta \frac{\mathbf{x}_\beta \times \mathbf{x}_\alpha}{(1-\mathbf{x}_\alpha\cdot\mathbf{x}_\beta)}, \quad (\alpha=1,\ldots,N), \tag{1}$$

where $\mathbf{x}_\alpha \in \mathbb{R}^3$ and $\|\mathbf{x}_\alpha\|=1$. The unit vector $\mathbf{x}_\alpha$ denotes the position of the αth vortex whose strength is given by $\Gamma_\alpha \in \mathbb{R}$. The relation with standard spherical coordinates on the unit sphere is given by

$$\mathbf{x}_\alpha = (\sin\theta_\alpha\cos\phi_\alpha, \sin\theta_\alpha\sin\phi_\alpha, \cos\theta_\alpha). \tag{2}$$

The prime on the summation indicates that the singular term $\beta=\alpha$ is omitted, and initially, the vortices are located at the given positions $\mathbf{x}_\alpha(0)\in\mathbb{R}^3$. The denominator in Eq. (1) is the intervortical distance, $l_{\alpha\beta}$, between vortex Γ_α and Γ_β since $l_{\alpha\beta}^2 \equiv \|\mathbf{x}_\alpha-\mathbf{x}_\beta\|^2 = 2(1-\mathbf{x}_\alpha\cdot\mathbf{x}_\beta)$. As described in Ref. 18, Eq. (1) has two conserved quantities associated with it, the Hamiltonian energy,

$$H = -\frac{1}{4\pi}\sum_{\alpha<\beta}^{N}\Gamma_\alpha\Gamma_\beta \log\|\mathbf{x}_\alpha-\mathbf{x}_\beta\|, \tag{3}$$

and the center-of-vorticity vector,

$$\mathbf{J} = \sum_{\alpha=1}^{N}\Gamma_\alpha\mathbf{x}_\alpha = \left(\sum_{\alpha=1}^{N}\Gamma_\alpha x_\alpha, \sum_{\alpha=1}^{N}\Gamma_\alpha y_\alpha, \sum_{\alpha=1}^{N}\Gamma_\alpha z_\alpha\right) = (J_x, J_y, J_z). \tag{4}$$

As shown in Ref. 18, for a nondegenerate relative equilibrium ($\|\mathbf{J}\|\neq 0$), the configuration rotates about the **J**-vector with frequency proportional to $\|\mathbf{J}\|$. In this paper, the alignment of **J** with respect to the axis of rotation of the sphere is crucial toward determining the existence conditions for vortex streets. Our formulation relies on the evolution equations for the relative distances (see Ref. 19),

$$\pi\frac{d(l_{\alpha\beta}^2)}{dt} = \sum_{\gamma=1}^{N}{}''\Gamma_\gamma V_{\alpha\beta\gamma} d_{\alpha\beta\gamma}, \tag{5}$$

where $d_{\alpha\beta\gamma} \equiv [(1/l_{\beta\gamma}^2)-(1/l_{\alpha\gamma}^2)]$. Here the "$''$" means the summation excludes $\gamma=\alpha$ and $\gamma=\beta$. $V_{\alpha\beta\gamma}$ is the volume of the parallelepiped formed by the vectors $\mathbf{x}_\alpha, \mathbf{x}_\beta, \mathbf{x}_\gamma$:

$$V_{\alpha\beta\gamma} = \mathbf{x}_\alpha\cdot(\mathbf{x}_\beta\times\mathbf{x}_\gamma) \equiv \mathbf{x}_\beta\cdot(\mathbf{x}_\gamma\times\mathbf{x}_\alpha) \equiv \mathbf{x}_\gamma\cdot(\mathbf{x}_\alpha\times\mathbf{x}_\beta).$$

Notice that the sign of $V_{\alpha\beta\gamma}$ can be positive or negative depending on whether the vectors form a right-or left-handed coordinate system. These equations of motion yield necessary conditions for relative equilibria,

$$\frac{d(l_{\alpha\beta}^2)}{dt} = 0, \quad \forall\,\alpha,\beta = 1\cdots N, \quad \alpha\neq\beta. \tag{6}$$

Using condition (6) in Eq. (5) gives the equation for the relative equilibria as fixed points of Eq. (5):

$$\sum_{\gamma=1}^{N}{}''\Gamma_\gamma V_{\alpha\beta\gamma} d_{\alpha\beta\gamma} = 0, \tag{7}$$

for each value of $\alpha,\beta=1,\ldots,N$. Based on the fact that Eq. (7) is linear in the vortex strengths, we write it as a linear matrix system

$$A\boldsymbol{\Gamma} = 0, \tag{8}$$

where $\boldsymbol{\Gamma}=(\Gamma_1,\Gamma_2,\ldots,\Gamma_N)^T\in\mathbb{R}^N$ is the vector of vortex strengths, and $A\in\mathbb{R}^{M\times N}$, $M=N(N-1)/2$, is the configuration matrix whose entries, given by the terms $V_{\alpha\beta\gamma}d_{\alpha\beta\gamma}$, encode the geometry of the configuration. Thus, to satisfy Eq. (8), we seek configurations for which

$$\det(A^T A) = 0, \tag{9}$$

in which case A is rank deficient, and has a nontrivial nullspace. We seek a basis set for this subspace of $\mathbb{R}^N$ from which we obtain the allowable vortex strengths.

This approach for identifying relative equilibria is ideally suited to the study of vortex street configurations on the sphere since N must necessarily be finite, and each of the intervortical distances have an upper bound given by the sphere diameter, see Fig. 1. By contrast, planar vortex streets are doubly infinite and thus require the summation of an infinite series to write the governing streamfunction (see, for example, Ref. 20). To adapt the configuration matrix approach in this setting would require that one make sense of the infinite dimensional configuration matrix that ensues.

C. SVD primer

Given the positions of the N-points, $\mathbf{x}_\alpha(0) \in \mathbb{R}^3$, $(\alpha = 1, \ldots, N)$ on the surface of the unit sphere, the configuration matrix $A \in \mathbb{R}^{M\times N}$ is obtained, with entries given by Eq. (7). The most general tool for characterizing the nullspace structure of the matrix is the singular value decomposition (SVD), which we briefly review. First, we find the eigenvalues $\lambda^{(i)}$ and eigenvectors $\mathbf{v}^{(i)}$ and $\mathbf{u}^{(i)}$ of the square covariance matrices $A^T A$ and AA^T, respectively (in practice, to compute the singular values, one does not take this approach as it is known to be numerically unstable):

$$(A^T A - \lambda^{(i)})\mathbf{v}^{(i)} = 0; \quad (AA^T - \lambda^{(i)})\mathbf{u}^{(i)} = 0. \tag{10}$$

The singular values $\sigma^{(i)}$ of A are related to $\lambda^{(i)}$ as follows: $\lambda^{(i)} = (\sigma^{(i)})^2$, and can be ordered from largest to smallest, $\sigma^{(1)} \equiv \sigma^{(\max)} \geq \sigma^{(2)} \geq \ldots \geq \sigma^{(\min)} \geq 0$. Then A has factorization $A = U\Sigma V^T$, where the first N columns of U are the left singular vectors $\mathbf{u}^{(i)} \in \mathbb{R}^M$ and the remaining $M-N$ columns are chosen to be orthonormal so that U is an orthogonal matrix, $U^T U = I$. Similarly, the N columns of V are the normalized right singular vectors $\mathbf{v}^{(i)} \in \mathbb{R}^N$, making V an orthogonal matrix, while the N singular values form the diagonal entries of $\Sigma \in \mathbb{R}^{M\times N}$ with zeroes off the diagonal. The right singular vectors, $\mathbf{v}^{(i)}$, corresponding to the *zero* singular values form an *optimal* basis set for the nullspace of A, and hence are used as a basis for the vortex strength vector $\boldsymbol{\Gamma}$, as seen in Eq. (8). Thus, the rank of A corresponds to the number of nonzero singular values, call this number $k \geq 0$. The factorization of A, written out via the SVD, is instructive:

$$A = \sum_{i=1}^{k} \sigma^{(i)} A^{(i)}, \tag{11}$$

where $A^{(i)} \equiv (\mathbf{u}^{(i)})(\mathbf{v}^{(i)})^T$ are each of rank one. Thus, the SVD expresses A as a linear combination of rank-one matrices, with relative weightings given by the nonzero singular values $\sigma^{(i)}$. Before detailing the streamline patterns, we focus first on the singular value distribution for the single VKS in the next section, as this will set the stage for determining all allowable vortex strengths for which the pattern remains in a vortex street formation, rotating about the polar axis.

II. SINGLE VON KÁRMÁN STREETS

A. No pole vortices

We first consider the simplest case of a single VKS consisting of two fixed latitudinal rings placed symmetrically across the equator at colatitudes $\phi = \phi_1$ and $\phi = \pi - \phi_1$, with n vortices per ring, evenly spaced. The vortices in the upper ring and those in the lower ring are skewed by half a wavelength with respect to each other as shown in Fig. 1. The longitudes associated with the n vortices in the upper ring are

$$\theta_\lambda = \frac{2\pi(\lambda - 1)}{n}, \quad (\lambda = 1, \ldots, n), \tag{12}$$

while those in the lower ring are

$$\theta_{\lambda+n} = \frac{2\pi(\lambda - 1)}{n} + \frac{\pi}{n}, \quad (\lambda = 1, \ldots, n). \tag{13}$$

It is now straightforward to produce the configuration matrix A associated with Eq. (8), given n. We take the simplest case with $n=2$, $N=4$ as an example. Equation (7) gives rise to the configuration matrix $A \in \mathbb{R}^{6\times 4}$:

$$A = \begin{bmatrix} 0 & 0 & 0 & 0 \\ 0 & -\alpha & 0 & -\alpha \\ 0 & \alpha & \alpha & 0 \\ \alpha & 0 & 0 & \alpha \\ -\alpha & 0 & -\alpha & 0 \\ 0 & 0 & 0 & 0 \end{bmatrix}; \qquad \alpha = \frac{(3\cos^2\phi_1 - 1)\cos\phi_1}{2(\cos^2\phi_1 + 1)}. \tag{14}$$

The covariance matrix is given by

$$A^T A = \begin{bmatrix} 2\alpha^2 & 0 & \alpha^2 & \alpha^2 \\ 0 & 2\alpha^2 & \alpha^2 & \alpha^2 \\ \alpha^2 & \alpha^2 & 2\alpha^2 & 0 \\ \alpha^2 & \alpha^2 & 0 & 2\alpha^2 \end{bmatrix}, \tag{15}$$

with $\det(A^T A) = 0$. The singular values for Eq. (14) can be obtained analytically (as square roots of the eigenvalues of the square covariance matrices):

$$\sigma^{(1)} = 2\alpha; \quad \sigma^{(2)} = \sigma^{(3)} = \sqrt{2}\alpha; \quad \sigma^{(4)} = 0. \tag{16}$$

With one singular value that is zero, the nullspace dimension is one, giving rise to a unique distribution of vortex strengths:

$$\mathbf{\Gamma} = \Gamma \begin{pmatrix} 1 \\ 1 \\ -1 \\ -1 \end{pmatrix}. \tag{17}$$

The first two components of the vector correspond to the upper (northern) ring, showing they must be equal. The second two components of equal but opposite strength vortices correspond to the lower (southern) ring. This is the general structure of the right singular vector of A for all n.

For example, the singular values (for a typical case $n=5$) are shown in Fig. 2. Note the fact that there is only one zero singular value, hence the nullspace dimension of A is one. The unique (up to multiplicative constant) nullspace vector is given by

$$\mathbf{\Gamma} = \Gamma \begin{pmatrix} 1 \\ \vdots \\ 1 \\ -1 \\ \vdots \\ -1 \end{pmatrix} \in \mathbb{R}^{2n}, \tag{18}$$

where the first set of n vortices of equal strength lie evenly spaced on the ring in the Northern hemisphere, while the second set of n equal but opposite strength vortices lie evenly spaced on the ring in the southern hemisphere. The center of vorticity, given by Eq. (4),

$$\mathbf{J} = \sum_{\alpha=1}^{N} \Gamma_\alpha \mathbf{x}_\alpha = 2N\Gamma \begin{pmatrix} 0 \\ 0 \\ \cos\phi \end{pmatrix}, \tag{19}$$

is aligned with the z-axis and the rings rotate around this axis.

B. With pole vortices

When two pole vortices are added to the system, there is a total of $N=2n+2$ point vortices. The singular value structure ($n=5$) is shown in Fig. 2(b), which should be compared with that without poles [Fig. 2(a)]. With the addition of pole vortices, the nullspace dimension increases from one to three. The basis set for the nullspace is most conveniently written:

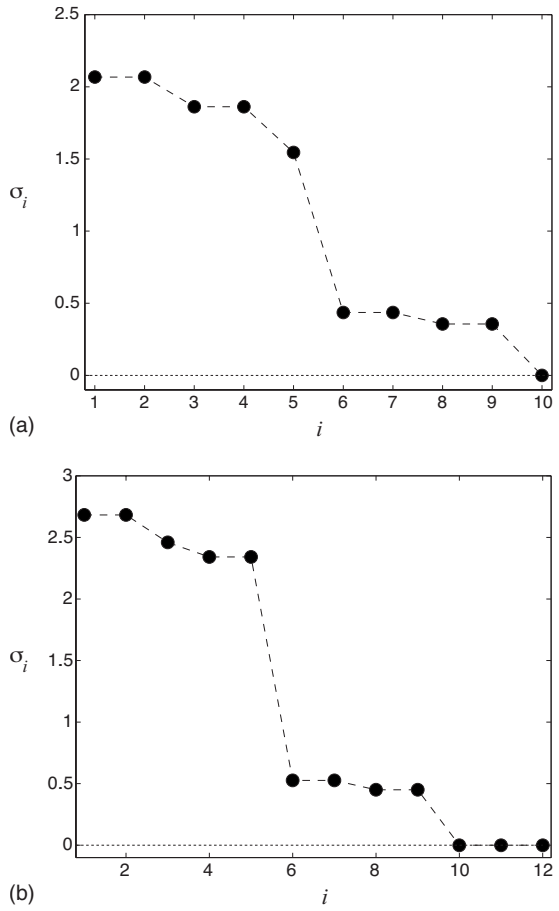

FIG. 2. Singular values for a single von Kármán vortex street with parameters $n=5$ and $\phi=3\pi/8$. (a) Without pole vortices, the nullspace dimension is one; (b) with pole vortices, the nullspace dimension is three.

$$\mathbf{\Gamma} = \Gamma \begin{pmatrix} 1 \\ \vdots \\ 1 \\ -1 \\ \vdots \\ -1 \\ 0 \\ 0 \end{pmatrix} + \Gamma_{\mathrm{np}} \begin{pmatrix} f(\phi_1) \\ \vdots \\ f(\phi_1) \\ 0 \\ \vdots \\ 0 \\ 1 \\ 0 \end{pmatrix} + \Gamma_{\mathrm{sp}} \begin{pmatrix} f(\phi_1) \\ \vdots \\ f(\phi_1) \\ 0 \\ \vdots \\ 0 \\ 0 \\ 1 \end{pmatrix} \in \mathbb{R}^{2n+2}. \tag{20}$$

The first n components of the first vector on the right correspond to the vortex strengths in the upper ring, the second n correspond to those in the lower ring. The last two vectors on the right tell us how the pole vortex strengths decompose in order for a relative equilibrium to exist with this configuration. The value Γ_{np} corresponds to the strength of the vortex at the north pole, while Γ_{sp} corresponds to that at the south pole. $f(\phi_1)$ is a general function of the ring latitude. The simplest case is when the pole vortices are equal and opposite, i.e., when $\Gamma_{\mathrm{np}}=-\Gamma_{\mathrm{sp}}=\Gamma_{\mathrm{p}}$. For this case, the nullspace dimension is 2, showing that the pole strength can be chosen independently from the ring strength. The vortex strength vector in this case reduces to

$$\mathbf{\Gamma} = \Gamma \begin{pmatrix} 1 \\ \vdots \\ 1 \\ -1 \\ \vdots \\ -1 \\ 0 \\ 0 \end{pmatrix} + \Gamma_p \begin{pmatrix} 0 \\ 0 \\ \vdots \\ \vdots \\ \vdots \\ 0 \\ 1 \\ -1 \end{pmatrix} \in \mathbb{R}^{2n+2}, \tag{21}$$

and the center of vorticity vector (4) in this case is aligned with the polar axis. The relative equilibrium in this case is a VKS rotating around **J**.

For the more general case in which $\Gamma_{np} \neq -\Gamma_{sp}$, it is readily seen that the vortex strength vector (20) gives rise to a decomposition in which the strength of those in the northern ring is not equal and opposite those in the southern ring. The configuration in this case is a relative equilibrium, but not a classical VKS. Thus, the only allowable arrangement which gives rise to a single VKS with pole vortices are those in which the poles are equal and opposite in strength and the northern ring is made up of vortices that are equal in strength, but opposite to those in the south.

C. Angular frequency formulas

To calculate the angular frequency of the vortex streets, we start with the equations of motion (1) written in spherical coordinates:[17]

$$\dot{\theta}_\alpha = \frac{1}{4\pi \sin \phi_\alpha} \sum_{\lambda \neq \alpha}^{N} \Gamma_\lambda \frac{\sin \phi_\alpha \cos \phi_\lambda - \cos \phi_\alpha \sin \phi_\lambda \cos(\theta_\alpha - \theta_\lambda)}{1 - \cos \gamma_{\alpha\lambda}}, \tag{22}$$

where $\cos \gamma_{\alpha\lambda} = \cos \phi_\alpha \cos \phi_\lambda + \sin \phi_\alpha \sin \phi_\lambda \cos(\theta_\alpha - \theta_\lambda)$. Since the vortex street rotates rigidly about the z-axis, it is sufficient to calculate the angular frequency, ω_n, for any of the vortices, hence, without loss of generality, we take $\alpha = 1$ with $N = 2n$ (no poles):

$$\omega_n \equiv \dot{\theta}_1 = \frac{1}{4\pi \sin \phi_1} \sum_{\lambda=2}^{2n} \Gamma_\lambda \frac{\sin \phi_1 \cos \phi_\lambda - \cos \phi_1 \sin \phi_\lambda \cos(\theta_1 - \theta_\lambda)}{1 - \cos \gamma_{1\lambda}}. \tag{23}$$

It is convenient to split the sum into two parts, first summing over the vortices in the upper ring where $\lambda = 2, \ldots, n$, $\phi_\lambda = \phi$, and $\Gamma_\lambda = 1$, then over those in the lower ring where $\lambda = n+1, \ldots, 2n$, $\phi_\lambda = \pi - \phi$, and $\Gamma_\lambda = -1$. Hence

$$\omega_n = \frac{1}{4\pi \sin \phi} \left[\sum_{\lambda=2}^{n} \frac{\sin \phi \cos \phi - \cos \phi \sin \phi \cos(\theta_1 - \theta_\lambda)}{1 - \cos^2 \phi - \sin^2 \phi \cos(\theta_1 - \theta_\lambda)} - \sum_{\lambda=n+1}^{2n} \frac{\sin \phi \cos(\pi - \phi) - \cos \phi \sin(\pi - \phi) \cos(\theta_1 - \theta_\lambda)}{1 - \cos \phi \cos(\pi - \phi) - \sin \phi \sin(\pi - \phi) \cos(\theta_1 - \theta_\lambda)} \right]. \tag{24}$$

Now, using the fact that $\cos(\pi - \phi) = -\cos \phi$, $\sin(\pi - \phi) = \sin \phi$, and Eqs. (12) and (13), which state that the n vortices are evenly spaced on each ring, with the lower ring skewed by π/n with respect to the upper ring, we obtain

$$\omega_n = \frac{\cos \phi}{4\pi \sin \phi} \left\{ \frac{(n-1)}{\sin \phi} + \sin \phi \sum_{\lambda=1}^{n} \frac{1 + \cos\left(\frac{2\pi(\lambda - 1)}{n} + \frac{\pi}{n} \right)}{1 + \cos^2 \phi - \sin^2 \phi \cos\left(\frac{2\pi(\lambda - 1)}{n} + \frac{\pi}{n} \right)} \right\}. \tag{25}$$

We show in Fig. 3 plots of ω_n versus ϕ for $n = 2, \ldots, 6$ for the full range $0 \leq \phi \leq \pi/2$. From Eq. (25), it is straightforward to show that $\omega_n \to \infty$ as $\phi \to 0$, corresponding to the limit in which all the vortices in the upper ring coalesce at the north pole, and all those in the lower ring coalesce at the south pole, and $\omega_n \to 0$ as $\phi \to \pi/2$, corresponding to the limit in which all the vortices are equally spaced along the equator, having alternating equal but opposite strength.

With the addition of pole vortices of strength $\Gamma_{np} \equiv \Gamma_p$ at the north pole, and $\Gamma_{sp} \equiv -\Gamma_p$ at the south pole, the VKS remains intact, but the angular frequency changes. Using Eq. (22) to calculate this change, we apply it with $\theta_\alpha = \theta$, $\phi_\alpha = \phi$, with one term in the sum, $N = 1$, corresponding to $\Gamma_\lambda = \Gamma_1 = \Gamma_p$ and $\phi_\lambda = \phi_1 = 0$ to obtain the effect from the vortex located at the north pole:

$$\omega_{np} = \dot{\theta} = \frac{\Gamma_p}{4\pi \sin \phi} \frac{\sin \phi}{1 - \cos \phi} = \frac{\Gamma_p}{4\pi(1 - \cos \phi)}. \tag{26}$$

Similarly, to obtain the effect from the south pole vortex, we use Eq. (22) with one term in the sum corresponding to $\Gamma_\lambda = \Gamma_1 = -\Gamma_p$ and $\phi_\lambda = \phi_1 = \pi$ to obtain the effect from the south pole vortex:

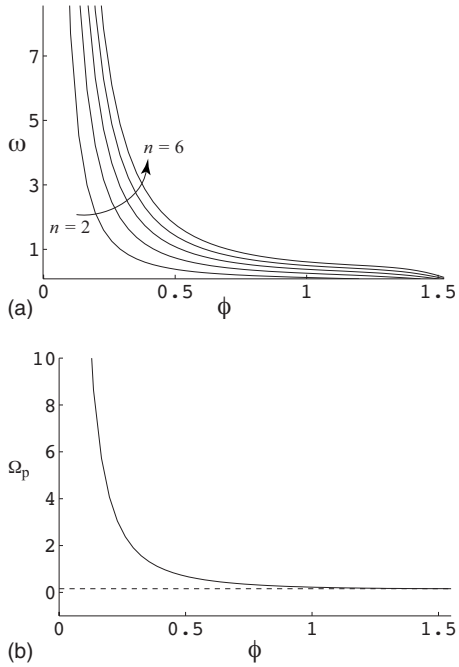

FIG. 3. (a) Angular velocity ω as a function of ϕ for a single VKS with $n=2\cdots6$. (b) Additional angular velocity Ω due to pole vortices with $\Gamma_p=+1$. As ϕ approaches $\pi/2$, $\Omega\to\Gamma_p/2\pi$.

$$\omega_{sp}=\frac{\Gamma_p}{4\pi(1+\cos\phi)}. \tag{27}$$

The angular frequency of the full vortex street with pole vortices, Ω, is then a linear superposition of the frequencies ω_n, ω_{np}, and ω_{sp}, which can be written as

$$\Omega=\omega_n+\Omega_p, \tag{28}$$

where

$$\Omega_p=\omega_{np}+\omega_{sp}=\frac{\Gamma_p}{4\pi(1-\cos\phi)}+\frac{\Gamma_p}{4\pi(1+\cos\phi)}=\frac{\Gamma_p}{2\pi\sin^2\phi} \tag{29}$$

is the pole component. We plot this component of angular frequency due to the poles in Fig. 3(b).

D. Streamline topologies

With these formulas in hand, we are now in a position to plot the full range of allowable streamline patterns for the single VKS, with and without pole vortices. For this, we move in the appropriate rotating frame of reference to render the relative equilibrium fixed, and we plot the streamline patterns in this frame as a function of colatitude ϕ. This full range of patterns is shown in Figs. 4–6.

Figure 4 shows the case of a single street with no pole vortices, through the full range of values $\phi=0\to\pi/2$. Our convention is to use clockwise orientation ($\Gamma<0$) of the vortices in the northern hemisphere and counterclockwise ($\Gamma>0$) in the southern hemisphere, in agreement with patterns described in Ref. 2. Aside from the two limiting (degenerate) cases $\phi=0,\pi/2$, there is only one topology type throughout

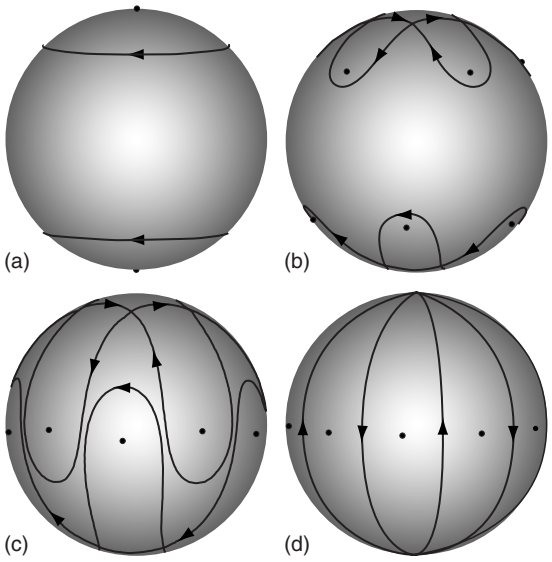

FIG. 4. Streamline topologies for a single VKS. The fixed parameters are $n=5$ and $\Gamma=-1$. The different topology types are obtained by varying ϕ. In (a), we begin with the degenerate case $\phi^*=0$, and in (d) we end with the degenerate case $\phi^*=\pi/2$. A single topology type exists in the range $0<\phi<\pi/2$, as illustrated in (b) and (c). We call these Type I topologies.

the entire range, which we call type I, shown in Figs. 4(b) and 4(c) at two different latitudes. The streamline pattern is topologically equivalent to that identified in Ref. 2 [their Fig. 3(b)], where a westward going jetstream meanders between the vortices comprising the street. The limiting case $\phi=0$ [shown in Fig. 4(a)] corresponds to the case of two vortices of equal and opposite strength $\pm n\Gamma$, located at the poles. For

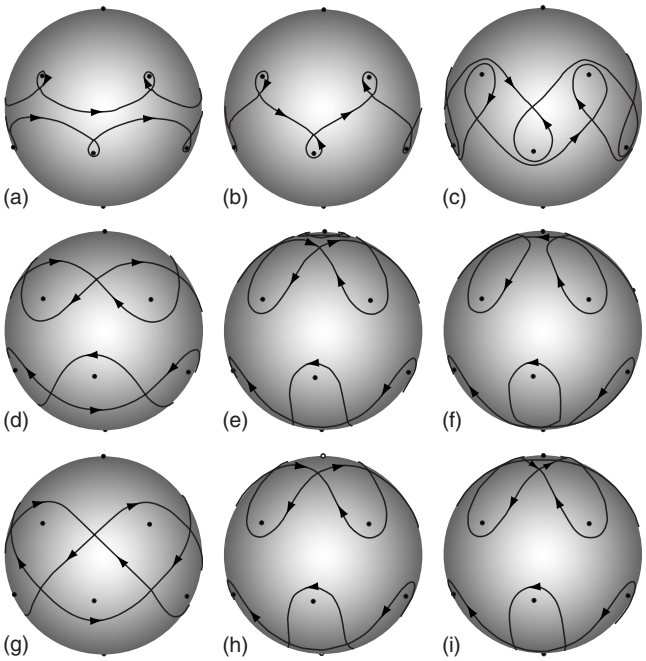

FIG. 5. Streamline topologies for a single VKS with vortices at the poles. The fixed parameters are $n=5$, $\Gamma=-1$, and $\phi=3\pi/8$. The different topology types are attained by varying Γ_p from 10 to -0.02. See Fig. 6 for a north pole view of the streamline topology bifurcations in the vicinity of $\Gamma_p^*=0$. (a) Type I; (b) $\Gamma_p^*=8$; (c) Type II; (d) $\Gamma_p^*=3.45$; (e) Type III; (f) $\Gamma_p^*=0$; (g) Type IV; (h) $\Gamma_p^*\approx-0.015$; (i) Type II.

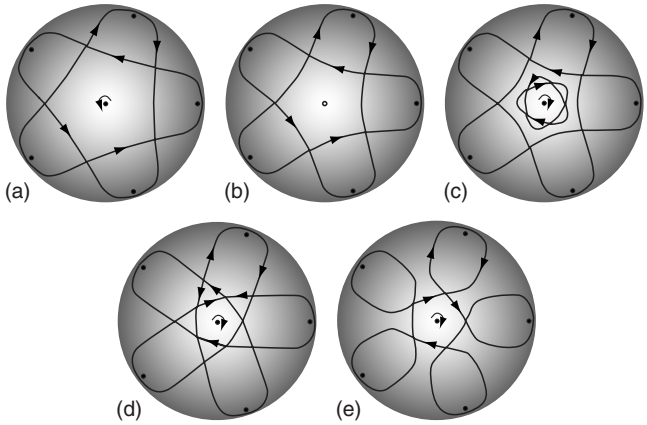

FIG. 6. North pole view of the streamline topologies for a single VKS with vortices at the poles. The fixed parameters are $n=5$, $\Gamma=-1$, and $\phi=3\pi/8$. Here, we illustrate the streamline topology bifurcations in the vicinity of $\Gamma_p^*=0$. In the range $0>\Gamma_p>-0.015$ as shown in (c), a flower-shaped contour consisting of five elliptic points and five saddle points appears about the pole. Figures 6(a)–6(e) correspond to Figs. 5(e)–5(i), respectively. (a) Type III; (b) $\Gamma_p^*=0$; (c) Type IV; (d) $\Gamma_p^*\approx-0.015$; (e) Type II.

this, the streamlines correspond to latitudinal lines. The other limiting case $\phi=\pi/2$ corresponds to the case of $2n$ point vortices evenly spaced along the equator, with alternating equal and opposite signs [see Fig. 4(d)].

In Fig. 5 we show the considerably richer set of patterns for a single street with pole vortices. In this panel, we fix the latitude at $\phi=3\pi/8$ and use the pole strength as our bifurcation parameter, ranging from $\Gamma_p=10\rightarrow-0.02$. The type I topology is shown first in Fig. 5(a). The first topological bifurcation occurs at value $\Gamma_p\approx8$, shown in Fig. 5(b). The new topology is then shown in Fig. 5(c), which we call type II. This is the topology identified in Ref. 2 [their Fig. 3(a)]. The next bifurcation occurs at $\Gamma_p\approx3.45$, shown in Fig. 5(d). This is the degenerate case shown in Ref. 2 [their Fig. 3(c)]. Shown in Fig. 5(e) is the next type III pattern, which corresponds to the pattern shown in Ref. 2 [their Fig. 3(b)]. Figure 5(f) shows the next bifurcation value which occurs when $\Gamma_p=0$, i.e., the pole vortex vanishes. After this (i.e., when the north pole strength becomes negative in sign), we obtain the topologies shown in Figs. 5(g)–5(i). Here, it is useful to view the streamline patterns looking down from the north pole, a view which is shown in the panel of Fig. 6. The structure of the streamline patterns is quite intricate here, particularly that identified as type IV, shown in Fig. 6(c). These are the full range of allowable patterns for the single street with pole vortices.

III. DOUBLE VON KÁRMÁN STREETS

The double VKS is considerably richer. We show the diagram in Fig. 7, both with and without pole vortices. The top northern ring is positioned at colatitude ϕ_1, while the lower northern ring, skewed with respect to the top, is positioned at colatitude ϕ_2. This arrangement is then reflected across the equator to the southern hemisphere. Thus, the two outermost rings are positioned at ϕ_1 and $\pi-\phi_1$, while the two innermost rings are at ϕ_2 and $\pi-\phi_2$.

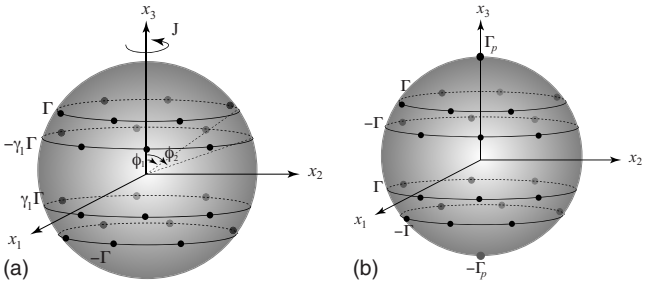

FIG. 7. Diagram of a double VKS with and without pole vortices. The configuration consists of one vortex street in the northern hemisphere, and a second in the southern hemisphere, where each street consists of two symmetrically skewed n-vortex rings. One ring in each hemisphere has a latitude of ϕ_1 from its respective hemisphere's pole; these are referred to as the ϕ_1-rings. The second ring in each hemisphere has an angle of ϕ_2, and these are referred to as the ϕ_2-rings.

A. The nullspace structure

In Fig. 8 we show the generic distribution of singular values, focusing on the case $n=5$. Figure 8(a) shows that in the case of no pole vortices, the nullspace dimension is one. The ϕ_1 rings have equal and opposite strengths $\pm\Gamma$, while the ϕ_2-rings have equal and opposite strengths $\pm\gamma_1\Gamma$, where

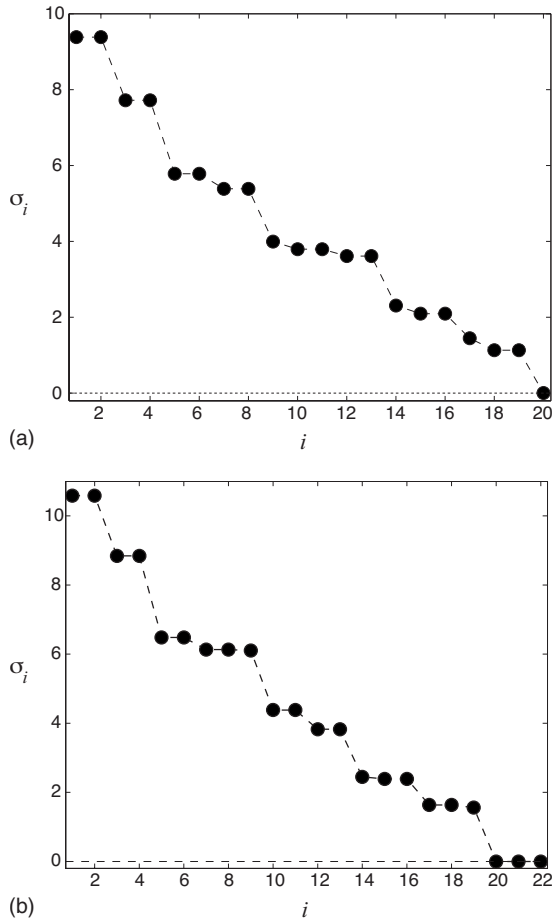

FIG. 8. Singular values for a double von Kármán vortex street: (a) without pole vortices and (b) with pole vortices. The fixed parameters are $n=5$, $\phi_1=13\pi/40$, and $\phi_2=3\pi/8$.

$\gamma_1 \in \mathbb{R}$. The vortices are ordered from the uppermost ring to the lowermost ring, namely,

$$\mathbf{\Gamma} = \Gamma(\underbrace{1, \ldots, 1}_{n}, \underbrace{-\gamma_1, \ldots, -\gamma_1}_{n}, \underbrace{\gamma_1, \ldots, \gamma_1}_{n}, \underbrace{-1, \ldots -1}_{n})^T \in \mathbb{R}^{4n}. \tag{30}$$

Unless $\gamma_1 = 1$, the configuration is not a double VKS.

With the addition of poles, the dimension of the null space is three, as shown in Fig. 8(b). The right null vector in this case, $\mathbf{\Gamma} \in \mathbb{R}^{4n+2}$, takes the general form

$$\mathbf{\Gamma} = \Gamma \begin{pmatrix} 1 \\ \vdots \\ 1 \\ -\gamma_1 \\ \vdots \\ -\gamma_1 \\ \gamma_1 \\ \vdots \\ \gamma_1 \\ -1 \\ \vdots \\ -1 \\ 0 \\ 0 \end{pmatrix} + \Gamma_{np} \begin{pmatrix} f_1 \\ \vdots \\ f_1 \\ f_2 \\ \vdots \\ f_2 \\ f_3 \\ \vdots \\ f_3 \\ 0 \\ \vdots \\ 0 \\ 1 \\ 0 \end{pmatrix} + \Gamma_{sp} \begin{pmatrix} g_1 \\ \vdots \\ g_1 \\ g_2 \\ \vdots \\ g_2 \\ g_3 \\ \vdots \\ g_3 \\ 0 \\ \vdots \\ 0 \\ 0 \\ 1 \end{pmatrix}. \tag{31}$$

We focus on the special case in which the poles are equal and opposite, hence $\Gamma_{np} = -\Gamma_{sp} \equiv \gamma_2 \Gamma$, and

$$\mathbf{\Gamma} = \Gamma \begin{pmatrix} 1 \\ \vdots \\ 1 \\ -\gamma_1 \\ \vdots \\ -\gamma_1 \\ \gamma_1 \\ \vdots \\ \gamma_1 \\ -1 \\ \vdots \\ -1 \\ 0 \\ 0 \end{pmatrix} + \Gamma \begin{pmatrix} \gamma_2(f_1 - g_1) \\ \vdots \\ \gamma_2(f_1 - g_1) \\ \gamma_2(f_2 - g_2) \\ \vdots \\ \gamma_2(f_2 - g_2) \\ \gamma_2(f_3 - g_3) \\ \vdots \\ \gamma_2(f_3 - g_3) \\ 0 \\ \vdots \\ 0 \\ \gamma_2 \\ -\gamma_2 \end{pmatrix} = \Gamma \begin{pmatrix} 1 + \gamma_2(f_1 - g_1) \\ \vdots \\ 1 + \gamma_2(f_1 - g_1) \\ -\gamma_1 + \gamma_2(f_2 - g_2) \\ \vdots \\ -\gamma_1 + \gamma_2(f_2 - g_2) \\ \gamma_1 + \gamma_2(f_3 - g_3) \\ \vdots \\ \gamma_1 + \gamma_2(f_3 - g_3) \\ -1 \\ \vdots \\ -1 \\ \gamma_2 \\ -\gamma_2 \end{pmatrix}. \tag{32}$$

From this representation, it is straightforward to choose variables so that the solution collapses into one dimension, namely,

$$\mathbf{\Gamma} = \Gamma(1, \ldots, 1, -1, \ldots, -1, 1, \ldots, 1, -1, \ldots, -1, \Gamma_p, -\Gamma_p)^T \in \mathbb{R}^{4n+2}, \tag{33}$$

where $\Gamma_p \equiv \gamma_2$. For this, we choose $f_1 = g_1$, $(f_2 - g_2) = -(f_3 - g_3)$, and $\gamma_1 = 1 + \gamma_2(f_2 - g_2)$. The center-of-vorticity vector then aligns with the polar axis:

$$\mathbf{J} = 2\Gamma \begin{pmatrix} 0 \\ 0 \\ n(\cos\phi_2 - \cos\phi_1) + \gamma_2 \end{pmatrix}, \tag{34}$$

and the system is a double VKS. We note that to achieve this relative equilibrium configuration requires a delicate balance of ring latitudes (ϕ_1, ϕ_2) and pole strengths γ_2. This balance is shown in Fig. 9 for a range of ratios $R = \phi_1/\phi_2$. In a sense, one can view the pole strength as the key parameter, which, if chosen judiciously, locks the double rings into a relative equilibrium much as the poles played an important role in the stability and bifurcations of a single latitudinal ring studied in Ref. 3. We show in Fig. 10 the angular velocity of the double street, with and without pole vortices, for a fixed value of ϕ_1, as a function of the ϕ_2 variable, for values of $n = 2, \ldots, 6$ (Fig. 10).

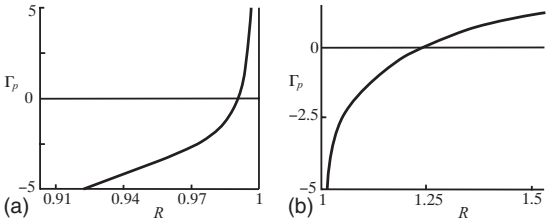

FIG. 9. Curves relating the pole vortex strength Γ_p vs the angle ratio $R = \phi_1/\phi_2$. The fixed parameters are $n=5$ and $\phi_1 = 3\pi/8$. (a) $\phi_1 < \phi_2 < \pi/2$ (i.e., $0.75 < R < 1$). (b) $0 < \phi_2 < \phi_1$ (i.e., $1 < R < +\infty$).

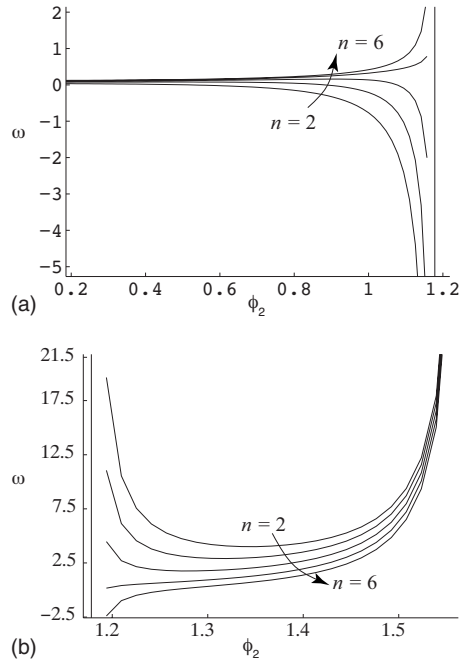

FIG. 10. Angular velocity ω as a function of ϕ_2 for $n = 2 \cdots 6$. The fixed parameter is $\phi_1 = 3\pi/8$. In (a), we illustrate the curves when $0 < \phi_2 < \phi_1$, while the curves in (b) correspond to $\phi_1 < \phi_2 < \pi/2$.

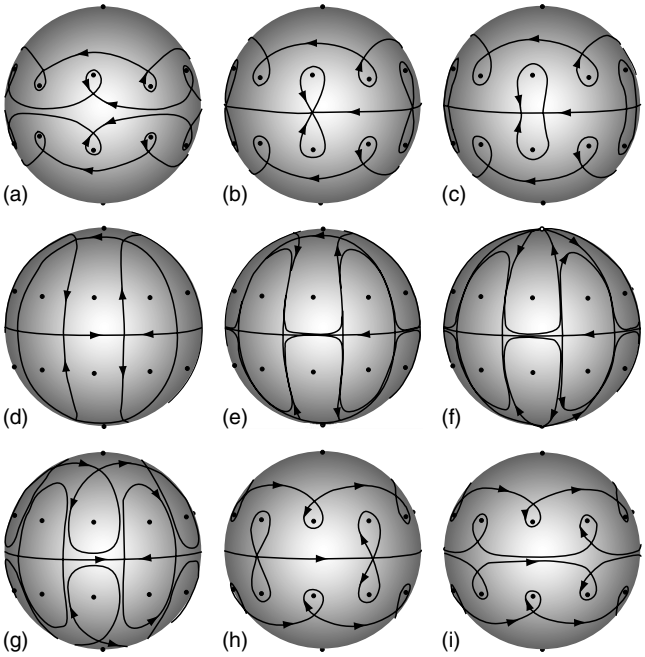

FIG. 11. Streamline topologies for a double VKS with vortices at the poles. The fixed parameters are $n=5$, $\phi_1=3\pi/8$, and $\Gamma=1$. The different streamline topologies are attained by varying ϕ_2. We use $R=\phi_1/\phi_2$, and R is increased from 0.9 to 0.996. The bifurcation point in (f) corresponds to the point at which $\Gamma_p=0$. See Fig. 12 for a north pole view of the streamline topology bifurcations in the vicinity of $\Gamma_p=0$. The topology types above correspond to all those observed in the range $\phi_1<\phi_2<\pi/2$ (i.e., $0.75<R<1$). (a) Type I; (b) $R^*\approx0.957$; (c) Type II; (d) $R^*\approx0.99065$; (e) Type III; (f) $R^*\approx0.990743$; (g) Type II; (h) $R^*\approx0.9953$; (i) Type I.

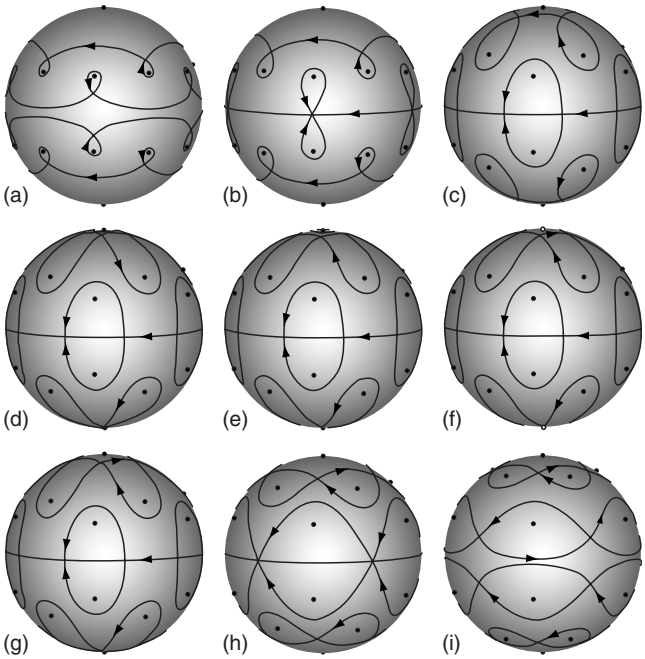

FIG. 13. A continuation of Fig. 11, the figures above are streamline topologies for a double VKS with vortices at the poles. The fixed parameters are again $n=5$, $\phi_1=3\pi/8$, and $\Gamma=1$. The different streamline topologies are attained by varying ϕ_2. We use $R=\phi_1/\phi_2$, and R is increased from 1.02 to 2. The bifurcation point in (f) corresponds to the point at which $\Gamma_p=0$. See Fig. 14 for a north pole view of the streamline topology bifurcations in the vicinity of $\Gamma_p=0$. The topology types above correspond to all those observed in the range $0<\phi_2<\phi_1$ (i.e., $1<R<+\infty$). (a) Type I; (b) $R^*\approx1.039$; (c) Type II; (d) $R^*\approx1.238$; (e) Type IV; (f) $R^*\approx1.23844$; (g) Type III; (h) $R^*\approx1.535$; (i) Type V.

B. Streamline topologies

In Figs. 11(a)–11(i) we show the full range of patterns obtained by varying ϕ_2 for fixed values of $\phi_1=3\pi/8$, $n=5$. We use the ratio $R\equiv\phi_1/\phi_2$ as our bifurcation parameter as it increases from $R=0.9$ [Fig. 11(a)] to $R=0.996$ [Fig. 11(i)]. We identify three distinct topology types: type I [Fig. 11(a)], type II [Fig. 11(c)], and type III [Fig. 11(e)]. The bifurcation values from one type to the next are also shown. Figure 12 shows a north pole view of the details of the topological bifurcation which takes place as the pole strength switches sign. In Fig. 13 we show the continuation of Fig. 11 for values $1.02\leq R\leq2.0$. Figure 14 shows details of the north pole view of the bifurcation when the pole strength changes sign.

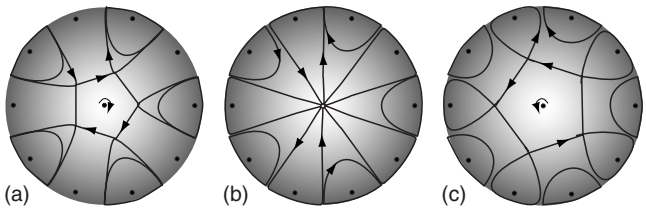

FIG. 12. North pole view of the streamline topologies for a double VKS with vortices at the poles in the vicinity of $R\approx0.990\,743$. At this point, the pole vortices switch signs. The fixed parameters are $n=5$, $\phi_1=3\pi/8$, and $\Gamma=1$. Figures 12(a)–12(c) correspond to Figs. 13(e)–13(g), respectively. (a) Type III; (b) $R^*\approx0.990743$; (c) Type III.

IV. DISCUSSION

The problem of how to place stacked latitudinal rings of evenly spaced point vortices on a sphere, together with the proper choice of vortex strengths in order that the system forms a relative equilibrium configuration, analogous to the

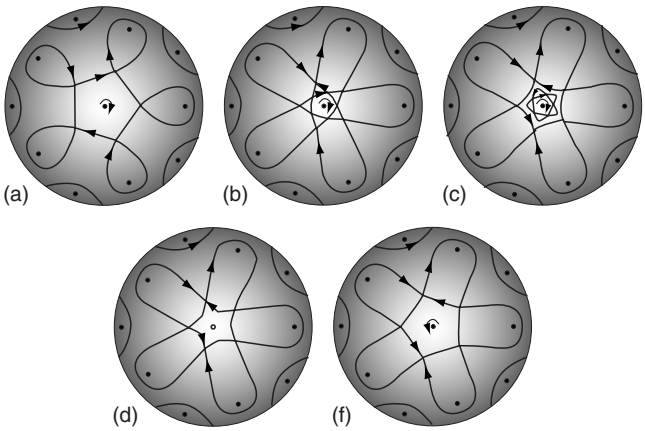

FIG. 14. North pole view of the streamline topologies for a double VKS with vortices at the poles in the vicinity of $R\approx1.238\,44$. At this point, the pole vortices switch signs. The fixed parameters are $n=5$, $\phi_1=3\pi/8$, and $\Gamma=1$. In the range $1.238<R<1.238\,44$ as shown in (c), a flower-shaped contour consisting of five elliptic points and five saddle points appears about the poles. (a) Type II; (b) $R^*\approx1.238$; (c) Type IV; (d) $R^*\approx1.23844$; (e) Type III. Figures 14(a)–14(e) correspond to Figs. 13(c)–13(g), respectively.

concentric ring problem in the plane discussed most completely in Ref. 21, is a delicate problem involving the simultaneous choice of latitudes, longitudes, and point vortex strengths. The configuration matrix approach used in this paper, which identifies the appropriate vortex strengths as elements of a nullspace associated with the matrix encoding the particular positions of the point vortices, seems ideally suited to handle the general problem. Maintaining such an equilibrium requires that the vortex strengths remain elements of the nullspace as the system evolves, and it is indeed remarkable that planetary atmospheres actually produce (approximately) such structures, which sometimes remain stable for decades (Refs. 2 and 8). The Hamiltonian stability theory for the VKS identified in this paper, an interesting and challenging problem in its own right, remains to be carried out.

[1]T. von Kármán, "Über den Mechanismus des Widerstands den ein bewegter Korper in einer Flüssigkeit erfährt," Göttingen Nachrichten, Math. Phys. Kl. **12**, 509 (1911).
[2]T. Humphreys and P. S. Marcus, "Vortex street dynamics: The selection mechanism for the areas and locations of Jupiter's vortices," J. Atmos. Sci. **64**, 1318 (2007).
[3]H. E. Cabral, K. E. Meyer, and D. S. Schmidt, "Stability and bifurcations for the $N+1$ vortex problem on the sphere," Regular Chaotic Dyn. **8**, 259 (2003).
[4]R. Kidambi and P. K. Newton, "Streamline topologies for integrable vortex motion on a sphere," Physica D **140**, 95 (2000).
[5]P. K. Newton and S. D. Ross, "Chaotic advection in the restricted four-vortex problem on a sphere," Physica D **223**, 36 (2006).
[6]M. Brøns, "Streamline topology: Patterns in fluid flow and their bifurcations," Adv. Appl. Mech. **41**, 1 (2007).
[7]M. Brøns, B. Jakobsen, K. Niss, A. V. Bisgaardt, and L. K. Voigt, "Streamline topology in the near wake of a circular cylinder at moderate Reynolds numbers," J. Fluid Mech. **584**, 23 (2007).
[8]P. S. Marcus, "Jupiter's great red spot and other vortices," Annu. Rev. Fluid Mech. **31**, 523 (1993).
[9]P. S. Marcus, "Prediction of global climate change on Jupiter," Nature (London) **428**, 828 (2004).
[10]A. Youssef and P. S. Marcus, "The dynamics of Jovian white ovals from formation to merger," Icarus **162**, 74 (2003).
[11]C. C. Lim, J. Montaldi, and M. Roberts, "Relative equilibria of point vortices on a sphere," Physica D **148**, 97 (2001).
[12]F. Laurent-Polz, "Point vortices on the sphere: A case with opposite vorticities," Nonlinearity **15**, 143 (2002).
[13]D. G. Crowdy, "Stuart vortices on a sphere," J. Fluid Mech. **498**, 381 (2004).
[14]D. Crowdy and M. Cloke, "Analytical solutions for distributed multipolar vortex equilibria on a sphere," Phys. Fluids **15**, 22 (2003).
[15]J. Y.-K. Cho and L. M. Polvani, "The emergence of jets and vortices in freely evolving shallow-water turbulence on a sphere," Phys. Fluids **8**, 1531 (1996).
[16]L. M. Polvani and D. G. Dritschel, "Wave and vortex dynamics on the surface of a sphere," J. Fluid Mech. **255**, 35 (1993).
[17]P. K. Newton, *The N-Vortex Problem: Analytical Techniques*, Appl. Math. Sci. Vol. 145 (Springer-Verlag, New York, 2001).
[18]P. K. Newton and H. Shokraneh, "The N-vortex problem on a rotating sphere. I. Multi-frequency configurations," Proc. R. Soc. London, Ser. A **462**, 149 (2006).
[19]M. I. Jamaloodeen and P. K. Newton, "The N-vortex problem on a rotating sphere. II. Heterogeneous platonic solid equilibria," Proc. R. Soc. London, Ser. A **462**, 3277 (2006).
[20]P. G. Saffman, *Vortex Dynamics* (Cambridge Univeristy Press, Cambridge, 1992).
[21]D. Lewis and T. Ratiu, "Rotating n-gon/kn-gon vortex configurations," J. Nonlinear Sci. **6**, 385 (1996).